Pergamon

Tetrahedron 58 (2002) 639–651

TETRAHEDRON

# Strong and directed association of porphyrins and iron(terpyridine)s using hydrogen bonding and ion pairing

Tyler B. Norsten, Kelly Chichak and Neil R. Branda*

*Department of Chemistry, University of Alberta, Edmonton, Alta., Canada T6G 2G2*

Received 8 June 2001; revised 29 August 2001; accepted 1 September 2001

**Abstract**—The combination of cooperative hydrogen bonding and ion pairing between cationic iron(II)terpyridines and anionic porphyrins yielded remarkably stable neutral complexes even in the highly competitive solvent DMSO. Isothermal titration calorimetry (ITC) was used to compare association constants, enthalpies and entropies of binding between various combinations of the two molecular components that make up the complexes. Steady-state luminescence studies highlighted that, as expected, the fluorescence quenching of the porphyrin is maximized in the cases where the iron(terpyridine) is strapped the tightest across the macrocycle. © 2002 Elsevier Science Ltd. All rights reserved.

## 1. Introduction

The efficient collection of solar energy is the primary task of natural light harvesting systems such as those found in plants, photosynthetic algae and cyanobacteria. These complicated photo-sensitive assemblies are responsible for initiating a cascade of energy and electron transfer reactions, ultimately affording usable forms chemical fuel. The key to the successful operation of these assemblies lies in their high degree of structural organization which ensures optimal alignment and relative proximity of the molecular components to maximize through-space communication of the chromophores. This refined architectural organization and structural integrity is a direct outcome of a multitude of contiguous non-covalent interactions.

With this in mind, significant efforts have been devoted to design and construct artificial multi-component photoactive arrays, particularly those involving porphyrins.[1–26] Because the photochemical behavior of the supramolecular assemblies will be dictated by their topology, design strategies must include judicial use of molecular recognition principles and, therefore, an emphasis on the logical programming of intermolecular attractions such as coordinative bonding,[2–12] ion pairing,[12–14] $\pi-\pi$ stacking[15] and hydrogen bonding[16–26] is paramount. Supramolecular systems that utilize only one of these interactions, however, do not take full advantage of the properties that each has to offer (expressed in their relative binding strength and directionality). Systems that fall into this category are often plagued by their functioning only in non-competitive solvents, or by the generation of assemblies with ill-defined topology and composition. The obvious answer to these problems is to design heterodiatopic or heteropolytopic building blocks where several different interactions are used in concert to guide the molecular recognition process and afford strong and selective complexation. The hydrogen bond is a particularly prized interaction used to unite building blocks due to its directionality and the fact that hydrogen bond donors and acceptors can be placed onto a building block with a high degree of precision. The utility of the hydrogen bond is greatly reduced, however, in polar competitive solvents that can better solvate the hydrogen bonding surface. The implementation of cooperative, ionic hydrogen bonding motifs, where the hydrogen bond partners are of opposite charge, can often overcome these destructive solvation effects.[27–31]

The formation of highly robust supramolecular assemblies is especially critical in order to investigate energy and electron transfer processes by luminescence spectroscopy. In the absence of strong complexation, excessive quantities of the quenching component must be added to produce the observable spectroscopic response at the low concentrations demanded by this analytical technique.

We have recently reported the self-assembly of a novel non-covalently united porphyrin–iron(II)terpyridine complex **1** and how the porphyrin's fluorescence is significantly quenched by the iron(terpyridine).[32] In the present article, we expand on the synthesis, structural characterization and luminescence properties of assembly **1** and its 1:2 counterpart **2**. We designed the building blocks in order to harness the beneficial recognition attributes of both ion pairing and

*Keywords*: hydrogen bond(s); luminescence quenching; molecular recognition, porphyrins; self-assembly.

* Corresponding author. Address: Department of Chemistry, Simon Fraser University, 8888 University Drive, Burnaby, BC, Canada V5A 1S6. Tel.: +1-604-291-3594; fax: +1-604-291-3765; e-mail: nbranda@sfu.ca

0040–4020/02/$ - see front matter © 2002 Elsevier Science Ltd. All rights reserved.
PII: S0040-4020(01)01096-1

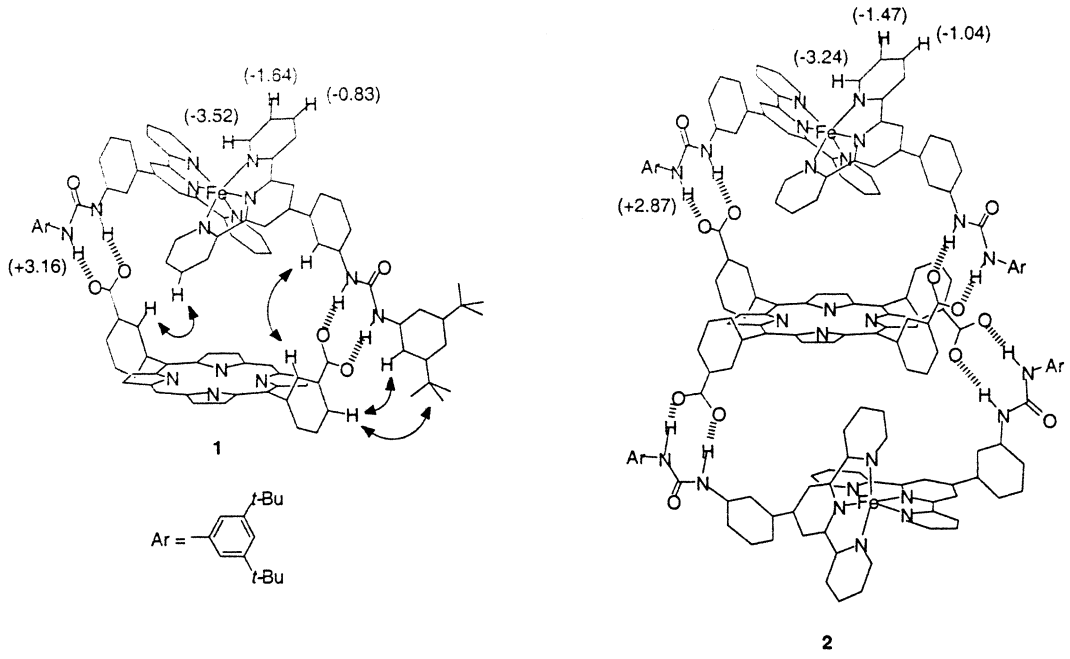


**Figure 1.** Schematic representation of complexes **1** and **2**. Observed intermolecular nOes (represented as arrows) and complexation-induced chemical shifts in the $^1$H NMR spectra (shown in parentheses) are highlighted. Double bonds and carbon-bound hydrogen atoms have been removed for clarity.

hydrogen bonding. The first interaction is provided by the attraction between the cationic iron(terpyridine) coordination compounds and the anionic porphyrinic carboxylates. The carboxylate groups on the porphyrins also act as charged hydrogen-bond-acceptor sites for the neutral bidentate urea hydrogen-bond-donors flanking the iron(terpyridine) component. The result is the self-assembly of the neutral complexes **1** and **2**, which retain both their structural integrity and topology even at low concentrations in the highly competitive solvent DMSO (Fig. 1).

## 2. Results and discussion

### 2.1. Synthesis of the molecular components

Terpyridine **5**[33] was prepared from *N*-(2-(pyridyl)-2-oxoethyl)pyridinium iodide (**3**) and (*E*)-3-(3‴-nitrophenyl)-1-(pyrid-2′-yl)prop-2-enone (**4**)[33] as shown in Scheme 1. Reduction of this product with $SnCl_2$, followed by subsequent dissymmertic urea formation employing 3,5-di-*tert*-butylaniline as the amine capping agent and triphosgene as the carbonyl linking agent conveniently yielded urea **6a**. Reacting urea **6a** with iodomethane in anhydrous DMF and in the presence of base cleanly afforded the *N*,*N*′-dimethylated analog **6b**, which will make its appearance as a control later in this report. The final iron(II) coordination compounds **7a** and **7b** were isolated as purple solids by treating 2 molar equivalents of **6a** and **6b** with 1 equiv. of $Fe(H_2O)_6(BF_4)_2$.

We also prepared the xanthene analog **13** in order to evaluate the effects (both structural and photophysical) of the relative proximity between the iron(terpyridine) and porphyrin components. The replacement of the 4′-phenyl ring in terpyridine **6a** by the extended xanthene skeleton in **12** provides a substantially deeper binding pocket (4–5 Å) in **13**, as compared to **7a** and, consequently, separates the two active components in space. The *meta*-substitution pattern between the terperidine and urea moieties is maintained across the xanthene backbone so as

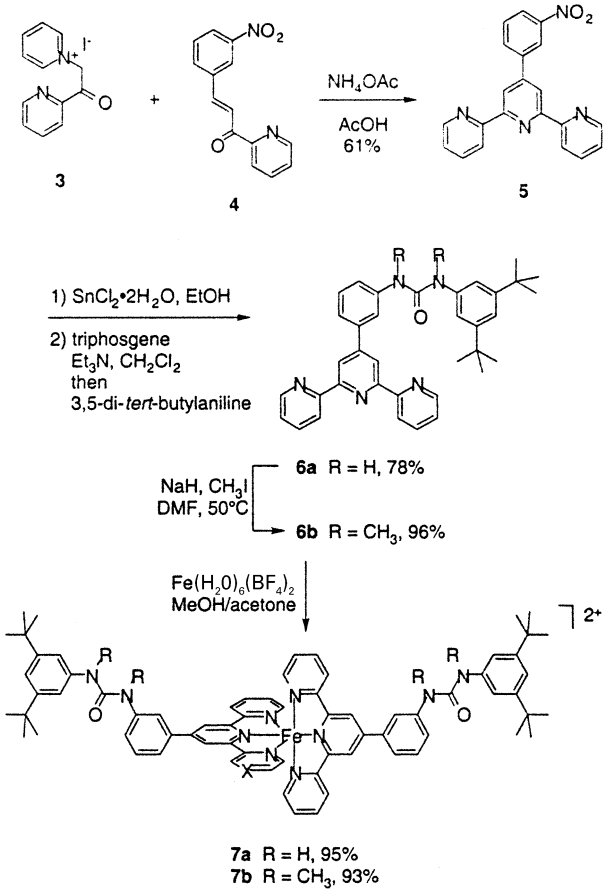


**Scheme 1.** Counterions for **7a** and **7b** are $BF_4^-$.

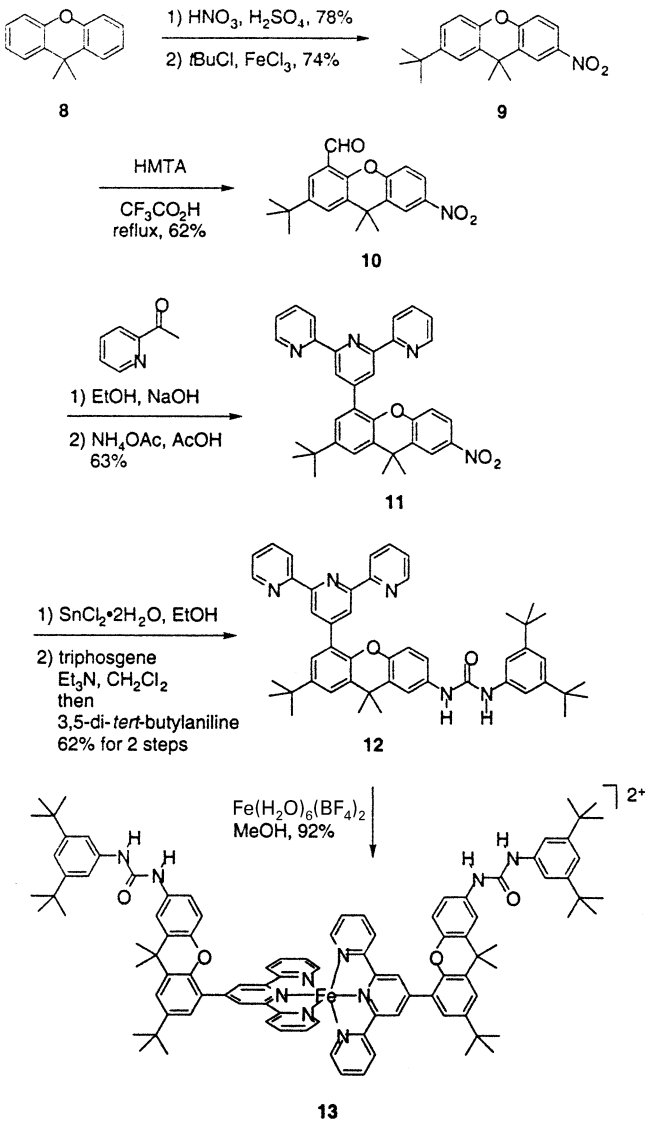


**Scheme 2.** Counterions for **13** are $BF_4^-$.

not to alter the hydrogen bonding vectors involved in the association between the two chromophores. The key intermediate is the dissymetric xanthene **9**, which was conveniently prepared by a two-step nitration-alkylkation procedure. The *tert*-butyl group's role was not to enhance solubility in organic solvents as is more typical of this group. (All studies will be performed using DMSO solutions, after all.) It was incorporated to block the more reactive *para*-site on the xanthene skeleton and direct the subsequent formylation reaction (**9**→**10**) to produce the desired substitution pattern. The aldehyde was transformed in two steps into terpyridine **11** by reacting it with an excess of 2-acetylpyridine and then with ammonium acetate. The conversion of **11** to **13** was accomplished in an identical fashion as already described for terpyridines **7a** and **7b** (Scheme 2).

All of the 5,15-*meso*-di-substituted porphyrins were synthesized by the acid-catalyzed cross-condensation[34] of the appropriately substituted benzaldehyde (**14a**[35] or **14b**) and dipyrrolemethane **15**[36] in $CH_2Cl_2$ (Scheme 3). The porphyrin esters (**16**) were saponified using KOH, followed by acidification to generate their corresponding carboxylic acids (**17**). The tertrabutylammonium carboxylate porphyrins **18a** and **18b** were generated by treating **17a** and **17b** with 2 equiv. of a methanolic solution of tetrabutylammonium hydroxide. The corresponding derivatives of 5,10,15,20-*meso*-tetra-substituted porphyrins **20a** and **20b** were generated from the known acids (**19a**[37] and **19b**[38]) employing 4 equiv. of a methanolic solution of tetrabutylammonium hydroxide (Scheme 4).

Hydrogen-bonded complexes **1** and **2** (Fig. 1) were prepared by simply mixing methanol solutions of porphyrin **18a** or **20a** with iron(terpyridine) **7a** in a 1:1 molar ratio for complex **1** and a 1:2 molar ratio for complex **2**. Complexes **1** and **2** precipitated from the reaction mixture and were easily isolated in high purity and in nearly quantitative yields. Because the association of the terpyridine and porphyrin components is accompanied by charge-balancing and the construction of neutral complexes, 2 and 4 equiv. of tetrabutylammonium tetrafluoroborate were also produced from the self-assembly reaction. These biproducts can be washed away during filtration.

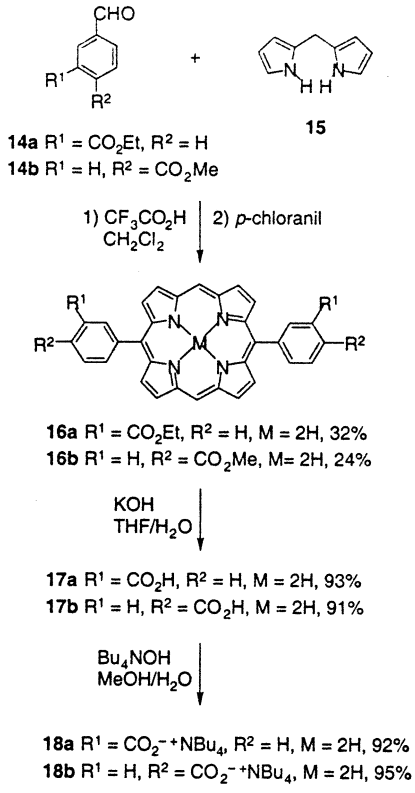


**Scheme 3.**

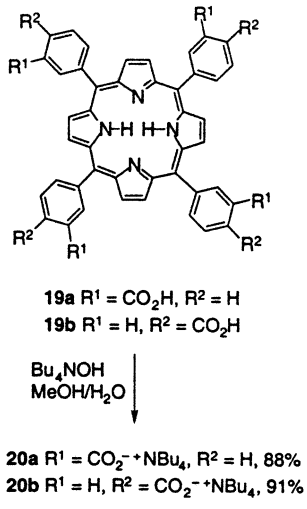


**Scheme 4.**

Molecular modeling[†] highlights the ideal lock-and-key fit between the two components making up complex **1** as well as the close proximity between them (Fig. 2). The importance of this spatial orientation and relative arrangement will become apparent throughout this report.

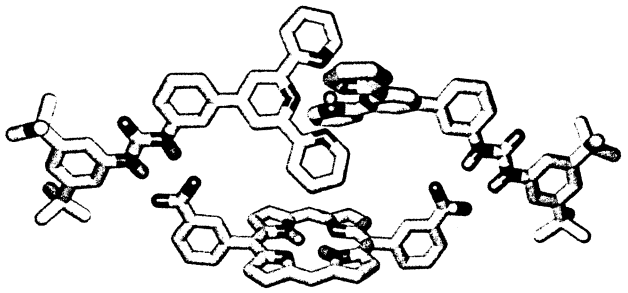

**Figure 2.** Optimized structure of complex **1** as predicted by molecular modeling.

## 2.2. $^1$H NMR characterization of the neutral complexes 1 and 2

Complexes **1** and **2** are reasonably soluble in highly polar solvents such as DMSO and DMF, but show poor solubility in other common organic solvents. The integration of the signals in the $^1$H NMR spectrum in DMSO-$d_6$ corresponding to the two components that make up complex **1** yielded a clean 1:1 stoichiometry attesting to the molecular composition of the complex.[‡] Upon association with the porphyrin, the signals for the protons on the terminal pyridine rings of **7a** shift significantly upfield while those for the N–H protons of the urea shift in the opposite direction (Fig. 3).

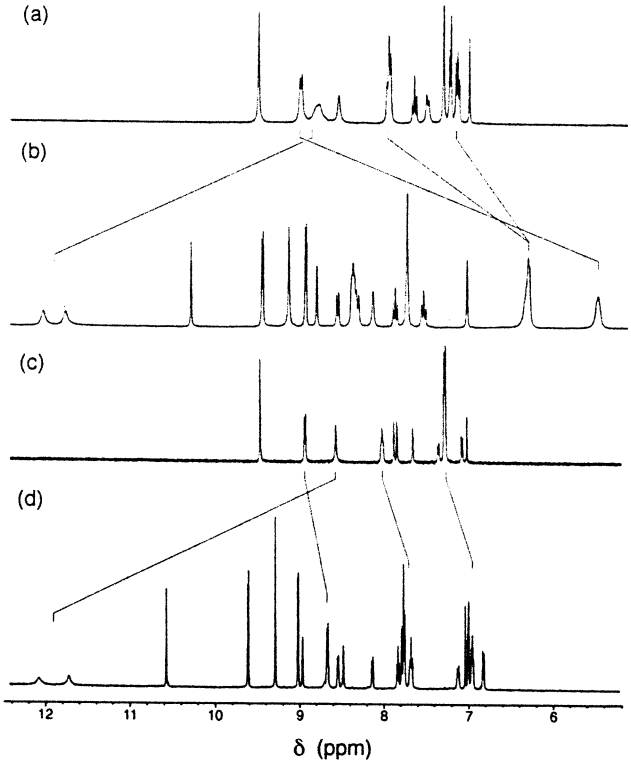


**Figure 3.** 300 MHz $^1$H NMR spectra of DMSO-$d_6$ solutions of: (a) iron(terpyridine) **7a**, (b) **7a**+porphyrin **18a**, (c) terpyridine **13**, and (d) **13**+porphyrin **18a**. CIS for selected hydrogen atoms are indicated by connecting lines.

[†] The starting geometry of the iron(terpyridine) component was obtained from the X-ray crystal structure of the 4-ethoxyphenyl analog of **7a** (see Supporting Information).

[‡] The stoichiometry of complexes **1** and **2** were confirmed using electrospray mass spectrometry, employing continuous infusion injection (see Section 4).

The $^1$H NMR complex-induced shift (CIS) values for the urea and selected terminal terpyridyl protons are shown in Fig. 1. The significant downfield shifts ($\Delta\delta$ greater than 3 ppm in DMSO-$d_6$) observed for the signals of the urea N–H protons are clearly a result of effective hydrogen bonding, even in such a polar and competitive solvent. The role of these hydrogen bonds is two-fold, one being to associate the two components. The second role is to steer the iron(terperidine) fragment into a position where it lies directly over the porphyrin plane. This guidance is successful as diagnosed by the upfield shifts observed for the hydrogen atoms lying directly over the porphyrin plane and, thus, within the strong shielding region of the macrocyclic ring. GCOSY and TROESY experiments aided in assigning the protons within complex **1**. Intermolecular nuclear Overhauser enhancements (nOes) (highlighted by the arrows in Fig. 1) support the claim that **7a** is strapped across the porphyrin ring and not straddling its side.

The signals for the hydrogen atoms on the terminal pyridine ring of the terpyridine ligand are unique in that they also appear as broad peaks in the spectrum (Fig. 3b). We attribute this to the fact that the strapped iron(terpyridine) fragment does not have the luxury to rotate freely above the porphyrin ring. The axis defined by the N–Fe–N bonds in **7a** is judged to be approximately 8.5 Å above the plane defined by the macrocycle which is not large enough to allow the terpyridine to pass over the porphyrin unencumbered. The result is that the terpyridine protons can range in distance from approximately 3.5 to 14.5 Å from the plane of the porphyrin at any given moment affording a variety of possible rotomers that can coexist within the NMR time-scale. Variable temperature NMR experiments failed to alter the shape of these broadened signals.

When the *para*-substituted porphyrin **18b** was exposed to iron(terpyridine) **7a**, a complex was isolated in a similar manner as already described for complex **1**. In this case, the hydrogen bonds are not suitably positioned to guide the formation of a strapped 1:1 complex, although the two components can certainly generate a polymeric array with the same 1:1 stoichiometry. The $^1$H NMR spectrum of this complex indeed indicated a 1:1 stoichiometry, however, the signals for the N–H protons of the urea only shift 1 ppm downfield. Also, there was no observable shifting of the terpyridine signals. These observations indicate that **7a** does not reside over the plane of porphyrin **18b** and instead suggests the existence of a polymeric aggregate $\mathbf{7a}_n\cdot\mathbf{18b}_m$. The relative positioning of the two chromophores and inability of **18b** to form cooperative hydrogen bonds with **7a** has a significant impact on the association between the two chromophores and the nature of the fluorescence quenching as will be discussed later.

The xanthene-modified iron(terpyridine) **13** provided us a suitable model compound to evaluate the rotation of the coordination compound over the plane of porphyrin **18a**. The $^1$H NMR spectrum of the resulting complex (Fig. 3d) shows a similar downfield shifting of the signals for the urea N–Hs of **13** upon complexation to **18a** as was already observed for **7a**. However, in this case, the signals corresponding to the hydrogen atoms on the terminal pyridine rings of **13** appear as sharp well-defined peaks that shift only slightly upfield. We attribute the sharpness of the signals to the fact that there is now adequate distance between the two chromophores to permit free rotation of the terpyridine rotor over the porphyrin plane. The reduced upfield shifting is easily ascribed to the fact that the pyridyl protons are lying further from the shielding region of the macrocycle.

The association of iron(terpyridine) **7a** with the tetra-substituted porphyrin **20a** resulted in the 1:2 complex **2**. Fig. 1 shows how, in this case, the two iron(terpyridine) units can alternately strap across opposing faces of one porphyrin macrocycle. The CIS values in the $^1$H NMR spectrum for the urea N–H and terpyridine protons are nearly identical to those of complex **1**. The only major difference is that the signals in the $^1$H NMR spectrum of **2** integrate for a 1:2 stoichiometry. The addition of 2 equiv. of **7a** to a methanol solution of the *para*-substituted porphyrinic analog **20b** resulted in a precipitate that was insoluble even in DMSO. Repeating the association experiment in DMSO-$d_6$ directly in an NMR tube resulted in an initial spectrum where the signals for the urea N–H protons shift 1.5 ppm downfield without any accompanying upfield shift of the signals for the terpyridyl protons. A precipitate formed in the NMR tube after several hours of standing. We suggest that the result of the association of **20b** and **7a** is a 1:2 complex where the two iron(terpyridine) fragments are strapped to the side of porphyrin **20b** (Fig. 4). This stoichiometry is supported by the calorimetric studies described later in this report.

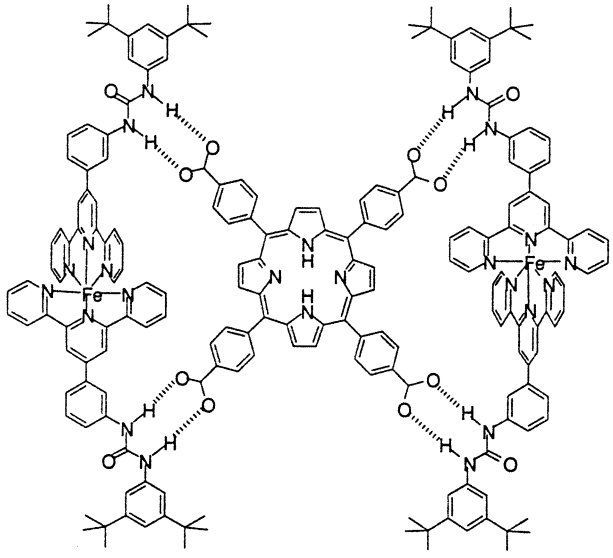

**Figure 4.** Proposed structure for the 2:1 complex formed when **7a** assembles with **20b**.

## 2.3. Stability of the complexes

The strength of the binding between iron(terpyridine) **7a** and porphyrins **18a** and **20a** was too large to be accurately measured by $^1$H NMR spectroscopy even in DMSO-$d_6$. The lack of any new or shifting absorption bands in the UV–Vis region of the spectrum during the formation of **1** or **2** also precluded this technique for the estimation of the association constants ($K_a$). Isothermal titration calorimetry (ITC),

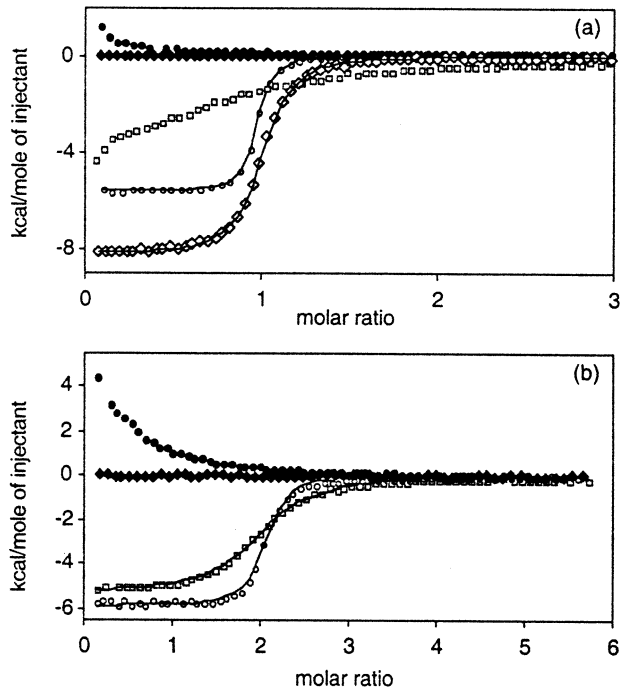


**Figure 5.** Heat change as iron(terpyridine)s **7a**,**b** and **13** are added to porphyrins **18a**,**b** and **20a**,**b** in DMSO: (a) **7a** into **18a** (○), **7b** into **18a** (●), **7a** into **18b** (□), **13** into **18a** (◇), and **7a** into DMSO (◆); (b) **7a** into **20a** (○), **7b** into **20a** (●), **7a** into **20b** (□) and **7a** into DMSO (◆). The solid lines represent the calculated isotherms.

between **18a** and **7a**[§]. Detailed calorimetric data for all titrations are collected in Table 1.

We argue that the reduced association between the two components in the corresponding xanthene complex **13**·**18a** is not due to any changes in hydrogen bonding, but instead, solely a result of changes in ion-paring and solvation. We feel comfortable with this claim because the hydrogen bonding sites in **7a** and **13** are virtually identical. One reason for the lower value of $K_a$ for **13**·**18a** may stem from a diminished attraction of the oppositely-charged ion pairs, as the two components are now forced to reside further away from each other. This should, however, afford a less negative enthalpic term for the binding of **13** by **18a** which was not observed (entries 1 and 3 in Table 1). An examination of the values of $\Delta S$ of association clearly shows that the difference in $K_a$ is entropically governed. The process of desolvation during a self-assembly reaction possesses an unfavorable enthalpic term (energy is required to break the bonds between the components and solvent molecules) and a favorable entropic term (there is an increase in disorder as solvent is released from the components). These arguments may apply to complexes **1** and **13**·**18a**, although the role of desolvation in such complicated systems is difficult to predict. We propose that, in the case of **13**·**18a**, because the two components are removed from each other in space, there are remaining solvent-accessible surfaces on both porphyrin faces and all around the iron(terpyridine) fragment. On the other hand, in **1** the two components are in direct contact and, in essence, solvate each other (at least on one face).

**Table 1.** Binding stoichiometries, association constants ($K_a$), association enthalpy ($\Delta H$) and association entropy ($\Delta S$) for the binding of porphyrins **18a**, **18b**, **20a**, and **20b** with iron(terpyridine)s **7a**,**c** and **13** in DMSO at 25°C

| Entry | Components | Stoichiometry[a] | $K_a$ ($M^{-1}$) | $\Delta H$ (kcal $mol^{-1}$) | $\Delta S$ (cal $mol^{-1}$ $deg^{-1}$) |
|---|---|---|---|---|---|
| 1 | **18a**[b]+**7a** | 1.1±0.1 | $2.5\times10^6\pm4.4\times10^5$ | −6.3±0.1 | 8.0±0.8 |
| 2 | **18b**[b]+**7a** | 1.0±0.1 | $3.0\times10^4\pm6.1\times10^3$ | −4.8±0.0 | 4.6±0.4 |
| 3 | **18a**[b]+**13** | 1.0±0.1 | $1.1\times10^6\pm3.0\times10^5$ | −8.4±0.2 | 0.3±0.2 |
| 4 | **20a**[c]+**7a** | 2.0±0.1 | $2.5\times10^6\pm3.2\times10^5$ | −5.9±0.1 | 9.5±0.4 |
| 5 | **20b**[c]+**7a** | 2.1±0.1 | $4.3\times10^5\pm2.2\times10^4$ | −5.4±0.1 | 7.6±0.3 |

The data represent average values from duplicate ITC experiments performed using fresh solutions. A typical experiments consisted of 60–70, 4 μL injections of a 1.45 mm solution of the terpyridine component into the calorimetry cell containing a 0.05 or 0.1 mM solution of the porphyrin component. A one-site binding model was employed for all data sets.

[a] Values represent equivalents of the terpyridine component per equivalent of the porphyrin component.

[b] [Porphyrin]=0.1 mM.

[c] [Porphyrin]=0.05 mM.

which measures the heat absorbed or evolved during a host–guest binding event, was employed to determine the thermodynamic parameters of the association of these high-affinity species. In addition to determining association constants, ITC conveniently provides the stoichiometry of binding as well as the enthalpy and entropy of association in a single experiment.

The integration of the heat generated as aliquots of iron(terpyridine) **7a** were added to a solution of porphyrin **18a** are plotted against the molar ratio generating the binding isotherm shown in Fig. 5a. This curve fit to a one-site binding model. The steep upward sigmoidal nature of the resulting curve inflecting at a molar ratio of 1 indicates that a strong exothermic association ($K_a=2.5\times10^6\pm4.4\times10^5$ $M^{-1}$) and 1:1 stoichiometry exists

When the hydrogen bonds are not suitably positioned to form a finite 1:1 complex, as is the case in the *para*-substituted porphyrin **18b**, the binding isotherm loses its sigmoidality and substantially flattens out. This clearly indicates that the lack of cooperative hydrogen bonding and the separation of the ion pairs in space results in a substantially weaker association between the molecular components (entry 2 in Table 1).

[§] It should be noted that the ITC data for the titrations of **18a** with **7a** do not rule out the possibility of higher-ordered equimolar aggregates (2:2, 3:3, etc.) which will all produce identical binding isotherms, although the $^1H$ NMR data clearly support the strapped 1:1 complex.

When hydrogen bonding is absent and association is purely ionic in nature, as is the case between porphyrin **18a** and the *N*,*N*′-dimethylated iron(terpyridine) **7b**, an endothermic isotherm was produced. This can be expected for ion pairing, where association is entropically driven with $\Delta H$ close to zero or positive. Attempts to fit the ITC data to a one-site binding model were unsuccessful and resulted in an undefined binding stoichiometry and an uncharacterizable and weak association. This behavior is likely a result of non-specific aggregation, typical of undefined ion pairing interactions. These data are consistent with previous ITC studies on non-specific solution based aggregation processes.[39]

The binding isotherm for porphyrin **20a** and **7a** were fit to a two-site binding model to yield the expected 1:2 stoichiometry and two similar association constants indicative of non-cooperativity (Fig. 5b and entry 4 in Table 1). It is not surprising that the two hydrogen-bond chelation sites in **20a** act independently as the binding of the iron(terpyridine) component on one face of the macrocycle is not expected to have any impact on the other.

The results of ITC experiment using the tetra-*para*-substituted porphyrin **20b** and **7a** also indicate the formation of a complex with a 1:2 stoichiometry (entry 5 in Table 1). Because the iron(terpyridine) fragment cannot strap across the face of the porphyrin macrocycle, as has already been proposed (see Fig. 4), the association between **20b** and **7a** is somewhat reduced as compared to the corresponding strapped complex **2**. This is surely due to a combination of a looser fit between **20b** and **7a** (adjacent carboxylate groups on the porphyrin do not completely span the receptor cleft provided by the **7a**), as well as, the fact that the hydrogen bonding vectors are slightly less than ideal (90° between adjacent carboxylates for **20b**, as opposed to the more ideal 60° angles for **20a**). The $\mathbf{7a}_2\cdot\mathbf{20b}$ structure proposed in Fig. 4 is supported by the increase in the value of $K_a$ for this complex as compared to that for **7a**·**18b** (entries 2 and 5 in Table 1) which proves some cooperative binding is taking place.

The data from the titration of **20a** with *N*,*N*′-dimethylated iron(terpyridine) **7c** could not be fit to the binding models again implying that an uncharacterizable, weakly-associated aggregate was produced from the self-assembly reaction as we have already argued for the association of **18a** with the same iron(terpyridine) component.

Two things are evident from our calorimetric studies: (1) ion pairing significantly contributes to the association between these anionic porphyrins and cationic iron(terpyridines), however, (2) complementary hydrogen bonding is ultimately responsible for the stoichiometic association and large exothermic response.

### 2.4. Fluorescence quenching behavior

The proximity and relative positioning of the two components within complexes **1** and **2** have a significant impact on the photophysical behavior of the final assemblies. Studies using steady-state fluorescence spectroscopy to monitor the changes in the emission intensities of DMSO solutions of **18a** and **20a** as the porphyrins were treated with aliquots of

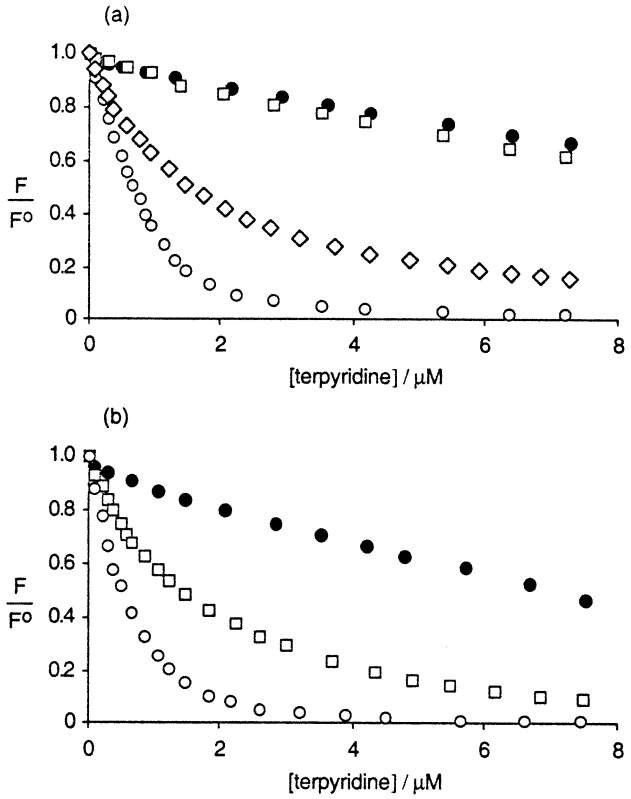


**Figure 6.** Inverse Stern–Volmer plots for fluorescence quenching titrations of (a) **18a** with **7a** (○), **18a** with **7b** (●), **18b** with **7a** (□) and **18a** with **13** (◇); ($\lambda_{ex}$=415 nm, $\lambda_{em}$=630 nm), and (b) **20a** with **7a** (○), **20a** with **7b** (●), and **20b** with **7a** (□); ($\lambda_{ex}$=430 nm, $\lambda_{em}$=650 nm). All titrations were preformed in DMSO. [porphyrin]=$1.0\times10^{-6}$ M, [iron(terpyridine)]=$2.0\times10^{-5}$ M.

**7a** are shown in Fig. 6.[¶] The immediate quenching of the fluorescence of **18a** is clearly a consequence of both the strong association and the intimacy of the two chromophores which ensures maximum through-space communication. The large extent of fluorescence quenching by **7a** as compared to its *N*,*N*′-dimethylated counterpart **7b**, which only slightly quenched the fluorescence of **18a** in a collision-dependant process, clearly indicates that an intra-complex quenching mechanism is in effect within **1**. Although still significant, the slightly reduced fluorescence quenching observed as xanthene **13** was added to porphyrin **18a** is most likely due to a combination of the weaker association between the two components and an increase in the distance between the two chromophores. Despite the fact that both hydrogen bonding and ion pairing are present in the $\mathbf{7a}_n\cdot\mathbf{18b}_m$ polymolecular assembly, the iron(terpyridine) fragment cannot form a cooperative hydrogen-bond strapped arrangement, resulting in reduced association between the molecular components and a significant lowering of the through-space communication between the chromophores. This is reflected in the titration of **18b** with **7a**.

[¶] The raw fluorescence data for the titration of **18a** with **7a** fit to 1:1 binding model and gave an association constant ($K_a$=$5.24\times10^6$ $M^{-1}$) that was close to that obtained for the calorimetry studies. The titration data was analyzed using Christopher A. Hunter's 1:1 complexation model program (Krebs Institute for Biomolecular Science, Department of Chemistry, University of Sheffield, UK).

A dramatic decrease in fluoresence was also observed when **7a** was titrated into a DMSO solution of porphyrin **20a**. When the *para*-substituted porphyrin **20b** was titrated with **7a**, the extent of quenching response was significantly reduced, and a much shallower quenching curve was produced. We attribute this to the fact that the iron(terpyridine) component can only bind onto the side of the porphyrin and not across its face. Consequently, the distance between the two chromophores in the proposed complex (Fig. 4) is greater than that in **2**.

When a sufficiently good electron acceptor is proximal, porphyrins are known to undergo rapid photoinduced electron transfer.[40] The result is a reduction in the observed fluorescence of the porphyrin because the photoexcited electron recombines with the porphyrin in a non-emitting pathway. Alternatively, the fluorescence of a porphyrin can be quenched in an energy transfer process.[41] This requires adequate overlap between the emission band of the photoexcited molecule and absorption band of the energy acceptor molecule. Because there is minimal overlap between the porphyrin emission band and the metal-to-ligand charge transfer (MLCT) absorption band of the iron(terpyridine) in the present systems (see Supporting Information), we believe that an energy transfer mechanism is not favorable, although, at this point, it cannot be completely ruled out.

## 3. Conclusions

These experiments clearly highlight the need to consider a polytopic approach in self-assembly synthesis, where the advantageous features of more than one type of molecular recognition interaction can be harnessed to provide access to robust and well-ordered supramolecular assemblies. In the present cases, ion pairing certainly contributes to the stability of complexes **1** and **2**, however, it is the cooperative hydrogen bonds that, not only aid in maintaining the structural integrity of the assemblies, but are the critical element necessary to align the building blocks into the optimal spatial arrangement so that the ion pairing attractive forces can be maximized. The complexes described in this report also represent attractive architectures to investigate the through-space communication of chromophores and the motion of the building blocks within the assemblies. The ability to fine tune the photonic and dynamic behavior of the supermolecules by modifying the chromophores (varying the metal within the metallo(terpyridine) and using a metalloporphyrin, for example) and/or by tailoring the size of the components (varying their proximity, for example) is paramount if supramolecular architectures are to be applied as the components of molecular machinery.

## 4. Experimental

### 4.1. General

All solvents (Caledon) were distilled prior to use with the exception of DMSO which was used as received. Solvents for NMR analysis (Cambridge Isotope Laboratories) were used as received. All synthetic precursors were purchased from Aldrich with the exception of aldehyde **14b** which was purchased from Acros.

$^1$H NMR characterizations were performed on a Varian Inova-500 instrument, working at 499.92 MHz, on a Varian Inova-400 instrument, working at 399.96 MHz, or on a Varian Inova-300 instrument, working at 299.96 MHz. Chemical shifts ($\delta$) are reported in parts per million relative to tetramethylsilane using the residual solvent peak as a reference standard. FT-IR measurements were performed using a Nicolet Magna-IR 750 spectrometer. UV–Vis absorption measurements were performed using a Varian Cary 400 Scan spectrophotometer. Low resolution mass spectrometry measurements were preformed using an Agilent Technologies 1100 MSD with an electrospray source. High resolution measurements were preformed using a Kratos MS-50 with an electron impact source or a PerSeptive Biosystems (Mariner) MS with an electrospray source. Solutions of complex **1**, **2**, and **13**·**18a** in 10% DMF/MeOH were prepared by dissolving the isolated complexes in a minimal amount of DMF and then diluting with methanol. These solutions were infused into the electrospray source (flow rate—30 μL/min, nebulizer pressure—12 psi). All other electrospray data were obtained by standard injection procedures.

### 4.2. Synthesis of iron(terpyridine)s

**4.2.1. Urea 6a.** Triphosgene (93 mg, 0.31 mmol) was added to a solution of 4′-(3‴-aminophenyl)-2,2′:6,2″-terpyridine[33] (302 mg, 0.93 mmol) and triethylamine (212 mg, 2.1 mmol) in freshly distilled $CH_2Cl_2$ (50 mL). After 2 h, 3,5-di-*tert*-butylamine (229 mg, 1.12 mmol) was added and the reaction stirred for an additional 2 h. The $CH_2Cl_2$ was removed under vacuum, the residue was dissolved in chloroform (100 mL), and shaken with 5% HCl (100 mL). The resulting yellow precipitate was washed several times with chloroform and then suspended in fresh chloroform (100 mL). The suspension was shaken with 5% NaOH (50 mL) and the layers separated. The resulting aqueous layer was extracted once with chloroform (50 mL) and the combined organic extracts were dried over $Na_2SO_4$. The chloroform was removed under vacuum and the resulting residue was triturated with a minimal amount of $CHCl_3$ (2×5 mL) and filtered yielding a white solid. The impure mother liquor was purified by column chromatography through alumina (Act II-III) using $CHCl_3$ as the eluent. Combined yield 78%; mp 236–237°C; $^1$H NMR (300 MHz, $CDCl_3$) $\delta$ 8.70 (m, 2H), 8.68 (s, 2H), 8.64 (d, $J$=7.2 Hz, 2H), 7.86 (dt, $J$=8.1, 1.8 Hz, 2H), 7.67–7.60 (m, 3H), 7.45 (t, $J$=8.1 Hz, 1H), 7.33 (dd, $J$=7.8, 4.8 Hz, 2H), 7.24 (m, 1H), 7.18 (d, $J$=1.2 Hz, 2H), 6.73 (br s, 1H), 6.41 (br s, 1H) 1.33 (s, 18H); $^{13}$C NMR (75 MHz, $CDCl_3$) $\delta$ 155.7, 154.9, 152.7, 150.7, 149.5, 149.4, 140.9, 138.8, 138, 137.5, 129.9, 124.5, 120.9, 120.2, 119.2, 117.8, 116.2, 115.9, 113.0, 34.5, 31.2; IR (microscope) $\nu$ 3332, 3155, 3054, 2963, 2904, 2867, 1651, 1607, 1586, 1567, 1441, 1287 cm$^{-1}$; HRMS (ES) Calcd for $[M+H]^+$ ($C_{36}H_{38}N_5O$) 556.3076. Found: 556.3076.

**4.2.2. *N*,*N*′-Dimethyled urea 6b.** A solution of **6a** (38.0 mg, 0.068 mmol) in anhydrous DMF (3 mL) was treated with NaH (8 mg, 0.33 mmol). After 15 min of

stirring at room temperature, iodomethane (12 μL) was added and the reaction stirred at 50°C under argon for 1.5 h. The reaction mixture was cooled to room temperature and $H_2O$ (10 mL) was added. The mixture was extracted with EtOAc (3×10 mL) and the combined organic extracts were dried over $Na_2SO_4$. The solvent was removed under reduced pressure and the residue was purified by column chromatography (1:1 hexane/EtOAc) through Alumina (Act II-III) affording a white solid. Yield 96%; $^1$H NMR (300 MHz, $CDCl_3$) $\delta$ 8.70 (m, 2H), 8.63 (d, $J$=8.1 Hz, 2H), 8.52 (s, 2H), 7.86 (dt, $J$=2.1, 7.5 Hz, 2H), 7.41 (d, $J$=7.5 Hz, 1H), 7.33 (ddd, $J$=7.5, 4.5, 0.9 Hz, 2H), 7.17 (s, 1H), 7.14 (t, $J$=7.5 Hz, 2H), 6.95 (dd, $J$=1.8, 1.8 Hz, 1H), 6.86 (d, $J$=7.8 Hz, 2H), 6.61 (d, $J$=1.8 Hz, 2H), 3.26 (s, 3H), 3.25 (s, 3H), 1.11 (s, 18H); $^{13}$C NMR (75 MHz, $CDCl_3$) $\delta$ 161.6, 156.2, 156.0, 151.3, 149.2, 146.5, 144.9, 139.1, 138.8, 129.0, 126.5, 124.5, 123.9, 121.3, 120.5, 119.3, 118.8, 39.7, 39.4, 34.7, 31.3; HRMS (EI) Calcd for $M^+$ ($C_{38}H_{41}N_5O$) 583.3311. Found: 583.3310.

**4.2.3. 9,9′-Dimethyl-3-nitro-xanthene.** A solution of 9,9′-dimethylxanthene (**8**) (2.1 g, 10.0 mmol) in glacial acetic acid (50 mL) was treated with fuming $HNO_3$ (700 mg) and fuming $H_2SO_4$ (1 mL). After stirring at room temperature for 2 h, the reaction mixture was poured over ice (200 mL) and neutralized by the careful addition of solid $NaHCO_3$. The mixture was extracted with $CH_2Cl_2$ (3×100 mL) and the combined organic extracts were dried over $Na_2SO_4$. The solvent was removed under vacuum and the residue purified by column chromatography through silca (50:1 hexane/EtOAc) affording a pale yellow solid. Yield 78%; mp 102–103°C; $^1$H NMR (300 MHz, $CD_2Cl_2$) $\delta$ 8.37 (d, $J$=2.7 Hz, 1H), 8.10 (dd, $J$=9.0, 2.7 Hz, 1H), 7.47 (dd, $J$=7.8, 2.7 Hz, 1H), 7.26 (ddd, $J$=7.2, 1.5, 0.6 Hz, 1H), 7.16 (td, $J$=7.5, 1.5 Hz, 1H), 7.16 (d, $J$=9.0 Hz, 1H), 7.10 (dd, $J$=7.8, 1.5 Hz, 1H), 1.68 (s, 6H); $^{13}$C NMR APT (125 MHz, $CD_2Cl_2$) $\delta$ 155.6 (C), 149.7 (C), 143.9 (C), 131.5 (C), 129.2 (C), 128.3 (CH), 126.7 (CH), 124.8 (CH), 123.8 (CH), 123.4 (CH), 117.5 (CH), 116.8 (CH), 34.7 (C), 32.8 ($CH_3$); IR (microscope) $\nu$ 3099, 2986, 2963, 2930, 2865, 2463, 2073, 1917, 1803, 1633, 1600, 1575, 1517, 1481, 1467, 1447, 1421, 1369, 1338, 1299, 1259, 1206, 1157, 1134, 1110, 1076, 1040 cm$^{-1}$; HRMS (EI) Calcd for $M^+$ ($C_{15}H_{13}NO_3$) 255.0895. Found: 255.0896.

**4.2.4. 6-*tert*-Butyl-9,9′-dimethyl-3-nitroxanthene (9).** A solution of 9,9′-dimethyl-3-nitroxanthene (1.91 g, 7.5 mmol) in $CH_2Cl_2$ (50 mL) was treated with *tert*-butyl chloride (694 mg, 7.5 mmol), followed by $FeCl_3$ (catalytic). After stirring at room temperature over night, the reaction was quenched by the addition of water (100 mL), extracted with $CH_2Cl_2$ and dried over $Na_2SO_4$. Recrystallization from EtOH afforded pale yellow crystals. Yield 74%; mp 162–168°C (decomp.); $^1$H NMR (300 MHz, $CD_2Cl_2$) $\delta$ 8.36 (d, $J$=2.7 Hz, 1H), 8.08 (dd, $J$=9.0, 2.7 Hz, 1H), 7.45 (d, $J$=2.1 Hz, 1H), 7.29 (dd, $J$=8.7, 2.1 Hz, 1H), 7.14 (d, $J$=9.0 Hz, 1H), 7.02 (d, $J$=9.0 Hz, 1H), 1.69 (s, 6H), 1.34 (s, 9H); $^{13}$C NMR APT (125 MHz, $CD_2Cl_2$) $\delta$ 155.8 (C), 147.7 (C), 147.4 (C), 143.8 (C), 131.6 (C), 128.3 (CH), 125.4 (CH), 123.7 (CH), 123.4 (CH), 123.2 (CH), 117.5 (CH), 116.2 (CH), 34.9 (C), 34.9 (C), 32.9 ($CH_3$), 31.6 ($CH_3$); IR (microscope) $\nu$ 3078, 2966, 2905, 2869, 1631, 1600, 1577, 1516, 1499, 1481, 1424, 1407, 1395, 1386, 1362, 1330, 1307, 1295, 1266, 1212, 1146, 1123, 1110, 1088, 1076 cm$^{-1}$; HRMS (EI) Calcd for $M^+$ ($C_{19}H_{21}NO_3$) 311.1521. Found: 311.1513.

**4.2.5. 3-*tert*-Butyl-9,9′-dimethyl-6-nitro-xanthene carboxaldehyde (10).** Hexamethylenetetraamine (HMTA) (491 mg, 3.5 mmol) was added in one portion to a solution of xanthene **9** (934 mg, 3.0 mmol) in $CF_3CO_2H$ (10 mL). After heating at reflux for 24 h, the reaction was cooled and poured into 4 M HCl (100 mL). After stirring at room temperature for 15 min, the mixture was extracted with $CH_2Cl_2$ (3×100 mL), the combined organic extracts were dried over $Na_2SO_4$ and the solvent evaporated under vacuum. Purification by column chromatography through silica ($CH_2Cl_2$) afforded a white solid. Yield 628 mg (62%); mp 237–239°C; $^1$H NMR (300 MHz, $CD_2Cl_2$) $\delta$ 10.66 (s, 1H), 8.40 (d, $J$=2.7 Hz, 1H), 8.14 (dd, $J$=9.0, 2.7 Hz, 1H), 7.81 (d, $J$=2.7 Hz, 1H), 7.74 (d, $J$=2.7 Hz, 1H), 7.27 (d, $J$=9.0 Hz, 1H), 1.72 (s, 6H), 1.36 (s, 9H); $^{13}$C NMR APT (125 MHz, $CD_2Cl_2$) $\delta$ 188.9 (CH), 154.6 (C), 149.6 (C), 147.6 (C), 144.4 (C), 131.4 (C), 129.9 (CH), 129.9 (C), 124.0 (CH), 123.9 (CH), 123.6 (C), 123.3 (CH), 117.8 (CH), 36.9 (C), 34.9 (C), 32.7 ($CH_3$), 31.3 ($CH_3$); IR (microscope) $\nu$ 3335, 3075, 2982, 2967, 2875, 2761, 1675, 1648, 1628, 1606, 1582, 1525, 1462, 1421, 1391, 1363, 1340, 1329, 1301, 1277, 1268, 1254, 1229, 1205, 1159, 1129, 1115, 1076 cm$^{-1}$; HRMS (EI) Calcd for $M^+$ ($C_{20}H_{21}NO_4$) 339.1471. Found: 339.1471.

**4.2.6. Nitroterpyridine 11.** A mixture of aldehyde **10** (250 mg, 0.737 mmol), 2-acetylpyridine (300 mg, 2.50 mmol), 5% aqueous NaOH (1 mL) and EtOH (3 mL) was stirred at room temperature for 15 h. The reaction was concentrated to dryness leaving a pink amphorous solid (385 mg). The pink solid (193 mg) was suspended in glacial acetic acid (1 mL), treated with excess $NH_4OAc$ (1 g) and heated at reflux for 15 h. The reaction was cooled and diluted with 50% aqueous EtOH, affording a yellow precipitate. The precipitate was collected by vacuum filtration and washed with 50% aqueous EtOH. Recrystallization from EtOH/$H_2O$ afforded an off-white solid. Yield 63%; mp 201–203°C; $^1$H NMR (300 MHz, $CD_2Cl_2$) $\delta$ 8.72 (m, 6H), 8.40 (d, $J$=2.4 Hz, 1H), 8.06 (dd, $J$=9.0, 2.7 Hz, 1H), 7.92 (td, $J$=7.5, 1.8 Hz, 2H), 7.58 (d, $J$=2.1 Hz, 1H), 7.50 (d, $J$=2.1 Hz, 1H), 7.38 (m, 2H), 7.11 (d, $J$=9.0 Hz, 1H), 1.77 (s, 6H), 1.41 (s, 9H); $^{13}$C NMR APT (125.7 MHz, $CD_2Cl_2$) $\delta$ 156.6 (C), 155.9 (C), 149.6 (CH), 148.1 (C), 147.7 (C), 144.8 (C), 144.0 (C), 137.2 (CH), 131.9 (C), 129.6 (C), 127.6 (C), 124.2 (CH), 123.8 (CH), 123.8 (CH), 123.1 (CH), 122.1, (CH), 121.5 (CH), 117.7 (CH), 35.4 (C), 35.1 (C), 32.4 ($CH_3$), 31.6 ($CH_3$); IR (microscope) $\nu$ 3062, 2963, 2869, 1728, 1627, 1605, 1582, 1567, 1542, 1524, 1489, 1468, 1440, 1420, 1388, 1364, 1342, 1266, 1226, 1215, 1173, 1117, 1089 cm$^{-1}$; HRMS (EI) Calcd for $M^+$ ($C_{34}H_{30}N_4O_3$) 542.2318. Found: 542.2315.

**4.2.7. 4′-(3-Amino-6-*tert*-butyl-9,9′-dimethylxanthyl)-2,2′:6′,2″-terpyridine.** $SnCl_2{\cdot}2H_2O$ (1.0 g, 4.5 mmol) was added to a hot (70–80°C) solution of terpyridine **11** (200 mg, 0.37 mmol) in absolute EtOH (30 mL). After stirring at 70–80°C for 2–3 h, the heat was removed and the reaction mixture was poured into an ice-cold mixture of

diethylenetriaminepentaacetic acid (DTPA) (2.3 g, 5.9 mmol) and $H_2O$ (100 mL). The mixture was neutralized with saturated $NaHCO_3$, the aqueous phase was extracted with $CHCl_3$ (3×50 mL), and the combined organic extracts were dried over $Na_2SO_4$. The chloroform was removed under vacuum yielding an off-white solid. The crude amine was carried on without further purification. Yield 96%; mp 130°C (decomp); $^1$H NMR (500 MHz, $CD_2Cl_2$) $\delta$ 8.73 (s, 2H), 8.71 (m, 4H), 7.91 (td, $J$=7.5, 1.5 Hz, 2H), 7.53 (d, $J$=2.5 Hz, 1H), 7.43 (d, $J$=2.0 Hz, 1H), 7.36 (m, 2H), 6.81 (d, $J$=9.0 Hz, 1H), 6.78 (d, $J$=3.0 Hz, 1H), 6.51 (dd, $J$=9.0, 2.5 Hz, 1H), 3.57 (br s, 2H), 1.67 (s, 6H), 1.40 (s, 9H); $^{13}$C NMR APT (125.7 MHz, $CD_2Cl_2$) $\delta$ 156.9 (C), 155.7 (C), 149.6 (CH), 148.8 (C), 146.7 (C), 145.7 (C), 144.0 (C), 142.9 (C), 137.1 (CH), 131.7 (C), 130.8 (C), 126.9 (C), 125.7 (CH), 124.0 (CH), 123.7 (CH), 122.2 (CH), 121.4 (CH), 117.3 (CH), 114.7 (CH), 112.2 (CH), 35.3 (C), 34.9 (C), 31.7 ($CH_3$), 31.7 ($CH_3$); IR (microscope) $\nu$ 3440, 3350, 3250, 3060, 2963, 2868, 1681, 1626, 1585, 1567, 1547, 1503, 1469, 1439, 1389, 1362, 1295, 1276, 1243, 1218, 1151, 1125, 1090 cm$^{-1}$; HRMS (EI) Calcd for $M^+$ ($C_{34}H_{32}N_4O$) 512.2576. Found: 512.2561.

**4.2.8. Terpyridine 12.** This urea was synthesized following the same procedure used to prepare **6a**. Purification by column chromatography (3:1 hexane/EtOAc) through Alumina (Act II-III) afforded a white solid. Yield 65%; mp 237–239°C; $^1$H NMR (500 MHz, $CD_2Cl_2$) $\delta$ 8.73 (s, 2H), 8.70 (m, 4H), 7.90 (td, $J$=7.5, 1.5 Hz, 2H), 7.53 (d, $J$=2.5 Hz, 1H), 7.48 (d, $J$=2.5 Hz, 1H), 7.45 (d, $J$=2.5 Hz, 1H), 7.35 (m, 2H), 7.20 (d, $J$=1.5 Hz, 2H), 7.18 (t, $J$=1.5 Hz, 1H), 7.14 (dd, $J$=9.0, 2.5 Hz, 1H), 6.95 (d, $J$=9.0 Hz, 1H), 6.81 (br s, 1H), 6.74 (br s, 1H), 1.67 (s, 6H), 1.39 (s, 9H), 1.29 (s, 18H); $^{13}$C NMR (125.7 MHz, $CD_2Cl_2$) $\delta$ 156.5, 155.2, 153.8, 152.2, 149.2, 148.5, 147.9, 145.8, 145.6, 137.2, 136.9, 132.9, 131.4, 129.8, 126.7, 125.6, 123.7, 123.1, 122.1, 121.7, 121.4, 119.9, 118.8, 117.5, 116.3, 35.0, 34.9, 34.7, 31.9, 31.6, 31.4; IR (microscope) $\nu$ 3321, 3064, 2963, 2926, 2867, 1650, 1604, 1585, 1567, 1501, 1469, 1439, 1411, 1391, 1363, 1275, 1245, 1224, 1090 cm$^{-1}$; HRMS (ES) Calcd for $[M+H]^+$ ($C_{49}H_{54}N_5O_2$) 744.4272. Found: 744.4282.

### 4.3. General metal-coordination procedure

$H_2O)_6(BF_4)_2$ (0.150 mmol) was added to a suspension of terpyridines **7a** and **7b** or **12** (0.30 mmol) in MeOH (50 mL). The mixture immediately turned purple yielding a homogenous solution, which was further stirred for 3 h at room temperature. The volume of MeOH was reduced to 5–10 mL, at which point 5–10 mL of $Et_2O$ was added affording a purple precipitate. The solid was isolated by filtration and washed times with cold acetone/$Et_2O$ (1:4).

**4.3.1. Compound 7a.** Prepared from **6a**. Yield 95%; $^1$H NMR (300 MHz, acetone-$d_6$) $\delta$ 9.55 (s, 4H), 9.06 (d, $J$=7.8 Hz, 4H), 8.70 (s, 2H), 8.51, (br s, 2H), 8.28 (br s, 2H), 8.07 (dt, $J$=7.8, 1.2 Hz, 4H), 7.95 (d, $J$=7.8 Hz, 2H), 7.64 (m, 8H), 7.52 (d, $J$=1.5 Hz, 4H), 7.27 (m, 4H), 6.90 (d, $J$=1.5 Hz, 4H), 1.34 (s, 36H); $^{13}$C NMR (75 MHz, acetone-$d_6$) $\delta$ 161.5, 159.3, 154.2, 153.8, 152.0, 151.9, 142.2, 140.2, 139.7, 138.3, 130.8, 128.5, 124.9, 122.5, 122.4, 121.5, 118.7, 117.3, 114.3, 35.5, 31.8; UV–Vis (DMSO) $\lambda_{max}$ (nm) (log $\epsilon$ ($M^{-1}$ cm$^{-1}$)) 279 (5.05), 288 (5.04), 328 (4.84), 573 (4.51); IR (microscope) $\nu$ 3381, 3078, 2962, 2904, 2867, 1698, 1606, 1548, 1495, 1440, 1396, 1298, 1217 cm$^1$; HRMS (ES) Calcd for $[M-2BF_4]^{2+}$ ($C_{72}H_{74}N_{10}O_2Fe$) 583.2667. Found: 583.2672.

**4.3.2. Compound 7b.** Prepared from **6b**. Yield 93%; $^1$H NMR (300 MHz, acetone-$d_6$) $\delta$ 9.58 (s, 4H), 8.99 (d, $J$=8.1 Hz, 4H), 8.07 (m, 8H), 7.48 (m, 6H), 7.29 (t, $J$=7.2 Hz, 4H), 7.22 (d, $J$=7.2 Hz, 2H), 7.12 (s, 2H), 6.90 (d, $J$=1.5 Hz, 4H), 3.36 (s, 6H), 3.29 (s, 6H), 1.25 (s, 36H); $^{13}$C NMR (75 MHz, acetone-$d_6$) $\delta$ 161.5, 160.8, 159.2, 153.8, 152.0, 150.8, 148.0, 146.0, 139.9, 137.3, 130.7, 128.6, 127.9, 125.1, 124.7, 124.2, 122.0, 120.8, 119.9, 39.8, 39.1, 35.4, 31.7; UV–Vis (DMSO) $\lambda_{max}$ (nm) (log $\epsilon$ ($M^{-1}$ cm$^{-1}$)) 289 (4.73), 326 (4.58), 576 (4.26); IR (microscope) $\nu$ 3080, 2962, 2902, 1662, 1617, 1593, 1541, 1447, 1409, 1287 cm$^{-1}$; HRMS (ES) Calcd for $[M-BF_4]^+$ ($C_{76}H_{82}N_{10}O_2Fe$ $BF_4$) 1309.6000. Found: 1309.6004.

**4.3.3. Compound 13.** Prepared from **12**. Yield 92%; $^1$H NMR (500 MHz, acetone-$d_6$) $\delta$ 9.60 (s, 4H), 8.98 (d, $J$=4.8 Hz, 4H), 8.27 (br s, 2H), 8.16 (br s, 2H), 8.10 (td, $J$=8.0, 1.5 Hz, 4H), 8.01 (d, $J$=2.5 Hz, 2H), 7.96 (d, $J$=2.5 Hz, 2H), 7.78 (d, $J$=2.0 Hz, 2H), 7.60 (d, $J$=4.5 Hz, 4H), 7.51 (dd, $J$=8.5, 2.5 Hz, 2H), 7.45 (d, $J$=2.5 Hz, 4H), 7.32 (ddd, $J$=8.0, 1.5, 1.5 Hz, 4H), 7.14 (t, $J$=1.5 Hz, 2H), 7.14 (t, $J$=2.5 Hz, 2H), 7.07 (d, $J$=9.0 Hz, 2H), 1.84 (s, 12H), 1.53 (s, 18H), 1.31 (s, 36H); $^{13}$C NMR APT (125 MHz, acetone-$d_6$) $\delta$ 161.0 (C), 159.5 (C), 154.1 (CH), 153.9 (C), 151.9 (C), 149.7 (C), 147.3 (C), 146.9 (C), 145.9 (C), 140.5 (C), 139.9 (CH), 137.4 (C), 131.8 (C), 131.1 (C), 128.5 (CH), 127.1 (CH), 126.6 (CH), 125.6 (CH), 125.5 (C), 124.8 (CH), 124.9 (CH), 119.5 (CH), 117.4 (CH), 117.2 (CH), 117.0 (CH), 114.1 (CH), 35.8 (C), 35.5 (C), 35.4 (C), 32.6 ($CH_3$), 31.9 ($CH_3$), 31.8 ($CH_3$); UV–Vis (DMSO) $\lambda_{max}$ (nm) (log $\epsilon$ ($M^{-1}$ cm$^{-1}$)) 278 (5.20), 327 (4.89), 570 (4.51); IR (microscope) $\nu$ 3388, 3076, 2963, 2906, 2868, 1694, 1608, 1552, 1503, 1453, 1415, 1363, 1277, 1246, 1213, 1059 cm$^{-1}$; HRMS (ES) Calcd for $[M-2BF_4]^{2+}$ ($C_{98}H_{106}N_{10}O_4Fe$) 771.3879. Found: 771.3861.

### 4.4. Synthesis of the porphyrins, general synthesis of porphyrinic esters 16a and 16b

$CF_3CO_2H$ (TFA) (1.25 equiv.) was added to a solution of ethyl 3-formylbenzoate (**14a**) or methyl 4-formylbenzoate (**14b**) (1.0 equiv.) and 2,2′-dipyrrolyl ketone **15**[36] (1.0 equiv.) in freshly distilled degassed $CH_2Cl_2$ (~5 mM). The reaction mixture was protected from light and stirred at room temperature for 18 h, at which time *p*-chloroanil (500 mg, 2.03 mmol) was added and the mixture was stirred for an additional 30 min. Triethylamine (3 mL) was added to neutralize the acid and the solution concentrated under vacuum to yield a purple residue. The crude residue was purified by column chromatography through silica by elution with $CHCl_3$, followed by trituration of the resulting purple solid with acetone.

**4.4.1. Compound 16a.** Yield 32%; $^1$H NMR (300 MHz, $CDCl_3$) $\delta$ 10.33 (s, 2H), 9.40 (d, $J$=4.8 Hz, 4H), 9.00 (d,

$J$=4.8 Hz, 4H), 8.94 (s, 2H), 8.51 (d, $J$=7.8 Hz, 2H), 8.43 (d, $J$=7.8 Hz, 2H), 7.88 (t, $J$=7.8 Hz, 2H), 4.48 (q, $J$=7.0 Hz, 4H), 1.41 (t, $J$=7.0 Hz, 6H), −3.14 (s, 2H); $^{13}$C NMR (75 MHz, $CDCl_3$) $\delta$ 166.9, 147.1, 145.5, 141.7, 138.7, 135.1, 132.0, 130.9, 129.6, 129.1, 127.2, 117.9, 105.6, 61.4, 14.4; UV–Vis ($CH_2Cl_2$) $\lambda_{max}$ (nm) (log $\epsilon$ ($M^{-1}\,cm^{-1}$)) 407 (5.67), 502 (4.32), 535 (3.78), 574 (3.80), 630 (3.30); IR (microscope) $\nu$ 3272, 3102, 2982, 2937, 2906, 1722, 1579, 1412, 1365, 1299, 1272, 1239 $cm^{-1}$; HRMS (EI) Calcd for $M^+$ ($C_{38}H_{30}N_4O_4$) 606.2269. Found: 606.2269.

**4.4.2. Compound 16b.** Yield 24%; $^1$H NMR (300 MHz, $CDCl_3$) $\delta$ 10.36 (s, 2H), 9.43 (d, $J$=4.8 Hz, 4H), 9.04 (d, $J$=4.8 Hz, 4H), 8.50 (d, $J$=8.1 Hz, 4H), 8.36 (d, $J$=8.1 Hz, 4H), 4.14 (s, 6H), −3.13 (s, 2H); $^{13}$C NMR (75 MHz, $CDCl_3$) $\delta$ 167.3, 146.7, 146.1, 145.3, 134.8, 132.0, 130.8, 129.6, 128.2, 117.9, 105.7, 52.5; UV–Vis (DMSO) $\lambda_{max}$ (nm) (log $\epsilon$ ($M^{-1}\,cm^{-1}$)) 408 (5.35), 503 (3.97), 538 (3.62), 574 (3.41), 629 (3.14); IR (microscope) $\nu$ 3247, 3093, 3035, 2957, 1719, 1606, 1433, 1312, 1293, 1266 $cm^{-1}$; HRMS (EI) Calcd for $M^+$ ($C_{36}H_{26}N_4O_4$) 578.1954. Found: 578.1967.

### 4.5. General synthesis of porphyrins 17a and 17b

An aqueous solution of KOH (4 mL, 2.0 M) was added to a solution of ester **16a** or **16b** (0.10 mmol) in THF (20 mL). After heating at reflux for 2–3 days, the mixture was cooled to room temperature and 5% HCl was added dropwise until the pH of the solution was 3–4. The resulting precipitate was filtered and triturated with $CH_2Cl_2$ yielding the pure porphyrin as a purple solid.

**4.5.1. Compound 17a.** Yield 93%; $^1$H NMR (300 MHz, DMSO-$d_6$) $\delta$ 13.27 (br s, 2H), 10.68 (s, 2H), 9.69 (d, $J$=4.5 Hz, 4H), 9.02 (d, $J$=4.5 Hz, 4H), 8.76 (s, 2H), 8.55 (d, $J$=7.8 Hz, 2H), 8.45 (d, $J$=7.8 Hz, 2H), 8.02 (t, $J$=7.8 Hz, 2H), −3.28 (s, 2H); UV–Vis (DMSO) $\lambda_{max}$ (nm) (log $\epsilon$ ($M^{-1}\,cm^{-1}$)) 408 (5.59), 502 (4.21), 538 (3.73), 574 (3.70), 629 (3.30); IR (microscope) $\nu$ 3277, 3200–2400, 1685, 1580, 1445, 1413, 1306, 1260, 1241 $cm^{-1}$; HRMS (ES-neg) Calcd for $[M-H]^-$ ($C_{34}H_{21}N_4O_4$) 549.1557. Found: 549.1555.

**4.5.2. Compound 17b.** Yield 91%; $^1$H NMR (300 MHz, DMSO-$d_6$) $\delta$ 10.68 (s, 2H), 9.68 (d, $J$=4.8 Hz, 4H), 9.05 (d, $J$=4.8 Hz, 4H), 8.43 (d, $J$=8.1 Hz, 4H), 8.41 (d, $J$=8.1 Hz, 4H), −3.27 (s, 2H); UV–Vis (DMSO) $\lambda_{max}$ (nm) (log $\epsilon$ ($M^{-1}\,cm^{-1}$)) 410 (5.35), 505 (3.97), 539 (3.64), 577 (3.48), 631 (3.20); IR (microscope) $\nu$ 3277, 3132, 1697, 1607, 1536, 1404, 1314, 1287, 1239, 1198, 1177, 1147, 1099 $cm^{-1}$; HRMS (ES-neg) Calcd for $[M-H]^-$ ($C_{34}H_{21}N_4O_4$) 549.1557. Found: 549.1561.

### 4.6. General synthesis of porphyrins 18a,b and 20a,b

A 0.1 M methanolic solution of tetrabutylammonium hydroxide was prepared fresh by diluting 652.9 mg of a 40% aqueous tetrabutylammonium hydroxide solution with methanol (10 mL). This solution (2 mL for **17a** and **17b**, and 4 mL for **19a**[37] and **19b**[38]) were added to the porphyrin (0.1 mmol) suspended in MeOH (2 mL). After stirring at room temperature for 16 h, the solvent was removed under vacuum affording a purple oil. This oil was dissolved in methanol (0.25–0.50 mL) and diethyl ether was added until the product oiled out. The supernatant was removed and discarded and the residue was dried under high vacuum for 1 day yielding a purple solid. The resulting porphyrinic salts can be stored for up to 6 months in an anhydrous environment of $CaSO_4$.

**4.6.1. Compound 18a.** Yield 95%; $^1$H NMR (300 MHz, $CDCl_3$) $\delta$ 10.62 (s, 2H), 9.64 (d, $J$=4.5 Hz, 4H), 9.03 (d, $J$=4.5 Hz, 4H), 8.67 (s, 2H), 8.29 (d, $J$=7.5 Hz, 2H), 8.13 (d, $J$=7.5 Hz, 2H), 7.73 (t, $J$=7.8 Hz, 2H), 3.15 (m, 16H), 1.55 (m, 16H), 1.29 (m, 16H), 0.92 (t, $J$=7.2 Hz, 24H), −3.22 (s, 2H); $^{13}$C NMR (75 MHz, $CDCl_3$) $\delta$ 171.6, 145.0, 139.9, 139.4, 135.8, 135.2, 131.5, 131.3, 129.1, 126.1, 120.0, 104.9, 58.7, 23.9, 19.6, 13.5; UV–Vis (DMSO) $\lambda_{max}$ (nm) (log $\epsilon$ ($M^{-1}\,cm^{-1}$)) 409 (5.49), 503 (4.27), 538 (3.87), 576 (3.79), 630 (3.41); IR (microscope) $\nu$ 3280, 3087, 2960, 2874, 1607, 1587, 1567, 1467, 1358, 1257 $cm^{-1}$; HRMS (ES-neg) Calcd for $[M-NBu_4]^-$ ($C_{50}H_{56}N_5O_4$) 790.4327, $[M+H-2NBu_4]^-$ ($C_{34}H_{21}N_4O_4$) 549.1557 Found: 790.4335, 549.1559.

**4.6.2. Compound 18b.** Yield 92%; $^1$H NMR (300 MHz, DMSO-$d_6$) $\delta$ 10.61 (s, 2H), 9.64 (d, $J$=4.5 Hz, 4H), 9.05 (d, $J$=4.5 Hz, 4H), 8.28 (d, $J$=7.8 Hz, 4H), 8.12 (d, $J$=7.8 Hz, 4H), 3.15 (m, 16H), 1.55 (m, 16H), 1.29 (m, 16H), 0.92 (t, $J$=7.2 Hz, 24H), −3.22 (s, 2H); UV–Vis (DMSO) $\lambda_{max}$ (nm) (log $\epsilon$ ($M^{-1}\,cm^{-1}$)) 410 (5.54), 504 (4.23), 540 (3.95), 579 (3.78), 633 (3.48); IR (microscope) $\nu$ 3279, 3111, 1703, 1605, 1586, 1402, 1239 $cm^{-1}$; HRMS (ES-neg) Calcd for $[M+H-2NBu_4]^-$ ($C_{34}H_{21}N_4O_4$) 549.1557. Found: 549.1560.

**4.6.3. Compound 20a.** Yield 91%; $^1$H NMR (300 MHz, DMSO-$d_6$) $\delta$ 8.82 (s, 8H), 8.21 (d, $J$=6.6 Hz, 8H), 8.04 ($J$=6.6 Hz, 8H), 3.14 (m, 32H), 1.55 (m, 32H), 1.26 (m, 32H), 0.92 (t, 48H), −2.89 (br s, 2H); UV–Vis (DMSO) $\lambda_{max}$ (nm) (log $\epsilon$ ($M^{-1}\,cm^{-1}$)) 421 (5.65), 518 (4.20), 552 (4.00), 593 (3.70), 648 (3.78); IR (microscope) $\nu$ 3466, 3277, 3089, 2960, 2873, 1666, 1595, 1551, 1483, 1367, 1280, 1239, 1150 $cm^{-1}$; HRMS (ES-neg) Calcd for $[M+2H-3NBu_4]^-$ ($C_{64}H_{65}N_5O_8$) 1031.4826, $[M+3H-4NBu_4]^-$ ($C_{48}H_{29}N_4O_8$) 789.2001, $[M+H-3NBu_4]^{2-}$ ($C_{64}H_{63}N_5O_8$) 514.7363, $[M+2H-4NBu_4]^{2-}$ ($C_{48}H_{28}N_4O_8$) 394.0956. Found: 1031.4839, 789.1980, 514.7344, 394.0959.

**4.6.4. Compound 20b.** Yield 88%; $^1$H NMR (300 MHz, DMSO-$d_6$) $\delta$ 8.79 (s, 8H), 8.62 (t, $J$=7.5, 4H), 8.25 (d, $J$=7.5 Hz, 4H), 8.14–8.04, (m, 4H), 7.65 (t, $J$=7.5 Hz, 4H), −2.86 (s, 2H); $^{13}$C NMR (300 MHz, $CDCl_3$) $\delta$ 171.5, 140.9, 138.9, 135.7, 134.9, 134.4, 129.1, 125.9, 125.8, 120.7, 118.2; UV–Vis (DMSO) $\lambda_{max}$ (nm) (log $\epsilon$ ($M^{-1}\,cm^{-1}$)) 422 (5.64), 518 (4.11), 553 (3.90), 591 (3.48), 648 (3.60); IR (microscope) $\nu$ 3318, 2961, 2874, 1607, 1588, 1566, 1486, 1370, 1252, 1158, 1109 $cm^{-1}$; MS (ES-neg) Calcd for $[M-NBu_4]^-$ ($C_{96}H_{134}N_7O_8$) 1514.0, $[M+H-2NBu_4]^-$ ($C_{80}H_{99}N_6O_8$) 1271.8, $[M+2H-3NBu_4]^-$ ($C_{64}H_{64}N_5O_8$) 1030.5. Found: 1514.0, 1271.7, 1030.4.

### 4.7. Synthesis of the terpyridine·porphrin complexes, general synthesis of complexes 1 and 2

A solution of iron(terpyridine) **7a** (0.024 mmol) in MeOH (12 mL) was added porphyrin **18a** (0.024 mmol) or **20a** (0.012 mmol). A dark precipitate immediately formed. After stirring at room temperature for 2–3 h, the solution was concentrated to 1–2 mL and filtered. The filter cake was washed several times with fresh MeOH affording a purple solid.

**4.7.1. Compound 1.** Yield 97%; $^1$H NMR (300 MHz, DMSO-$d_6$) $\delta$ 12.10 (br s, 2H), 11.84 (br s, 2H), 10.35 (s, 2H), 9.52 (d, $J$=4.8 Hz, 4H), 9.20 (s, 4H), 9.00 (d, $J$=4.8 Hz, 4H), 8.87 (s, 2H), 8.62 (d, $J$=7.5 Hz, 2H), 8.44 (m, 8H), 8.20 (s, 2H), 7.94 (t, $J$=7.8 Hz, 2H), 7.80 (s, 6H), 7.60 (t, $J$=7.8 Hz, 2H), 7.09 (s, 2H), 6.37 (br s, 8H), 5.55 (br s, 4H), 1.42 (s, 36H), −3.40 (s, 2H); MS (ES) Calcd for $[M+Na]^+$ ($C_{106}H_{94}N_{14}O_6FeNa$) 1738.9, $[M+2Na]^{2+}$ ($C_{106}H_{94}N_{14}O_6FeNa_2$) 880.9. Found 1738.7, 880.7.

**4.7.2. Compound 2.** Yield 95%; $^1$H NMR (300 MHz, DMSO-$d_6$) $\delta$ 11.95 (br s, 2H), 11.48 (br s, 2H), 9.27 (s, 8H), 8.75 (s, 8H), 8.59–8.51 (m, 16H), 8.29 (br s, 8H), 8.24 (d, $J$=7.5 Hz, 4H), 7.84 (d, $J$=7.5 Hz, 4H), 7.80 (t, $J$=7.5 Hz, 4H), 7.71 (s, 8H), 7.58 (t, $J$=7.5 Hz, 4H), 7.05 (s, 4H), 6.62 (br s, 8H), 6.54 (br s, 8H), 5.82 (br s, 8H), 1.37 (s, 72H), −3.06 (s, 2H); MS (ES) Calcd for $[M+2Na]^{2+}$ ($C_{192}H_{174}N_{36}O_{12}Fe_2Na_2$) 1583.7, Found: 1583.5.

**4.7.3. Xanthene complex 18a·13.** A solution of the iron-(terpyridine) **13** (0.002 mmol) in acetone (2 mL) was treated with porphyrin **18a** (0.002 mmol). The solution was stirred for 30 min and then sonicated for 10–20 s, at which point a dark precipitate formed. The suspension was filtered and the isolated solid was washed several times with acetone until the filtrate was colorless. Yield 91%; $^1$H NMR (500 MHz, DMSO-$d_6$) $\delta$ 12.14 (br s, 2H), 11.78 (br s, 2H), 10.62 (s, 2H), 9.65 (d, $J$=4.5 Hz, 4H), 9.32 (s, 4H), 9.04 (d, $J$=4.5 Hz, 4H), 8.91 (br s, 2H), 8.69 (d, $J$=7.5 Hz, 4H), 8.56 (d, $J$=8.0 Hz, 2H), 8.50 (br s, 2H), 8.15 (d, $J$=7.5 Hz, 2H), 7.85 (t, $J$=8.0 Hz, 2H), 7.78 (m, 8H), 7.70 (t, $J$=7.5 Hz, 4H), 7.13 (d, $J$=9.0 Hz, 2H), 7.05 (s, 2H), 7.01 (two br s, 4H), 6.96 (t, $J$=5.0, Hz, 4H), 6.82 (d, $J$=9.0 Hz, 2H), 1.78 (s, 12H), 1.47 (s, 18H), 1.41 (s, 36H), −3.27 (br s, 2H); MS (ES) Calcd for $[M+Na]^+$ ($C_{132}H_{126}N_{14}O_8FeNa$) 2115.4, $[M+2Na]^+$ ($C_{132}H_{126}N_{14}O_8FeNa_2$) 1069.2. Found: 2115.8, 1069.0.

### 4.8. Isothermal titration calorimetry

All binding experiments were preformed on an isothermal titration calorimeter from Microcal Inc. (Northampton, Massachusetts). In a typical ITC experiment, a 0.10 mM solution of the porphyrin dissolved in DMSO was added to the calorimetry cell (volume=1.448 mL). A 1.45 mM solution of the iron(terpyridine) in DMSO was introduced in 60, 4 μL injections (4 min between injections) until a total of 240 μL of iron(terpyridine) was added. The solution was maintained at a constant operating temperature of 25°C and continuously stirred (400 rpm) to ensure rapid mixing. The data from the resulting injections were evaluated using a one- or two-site non-linear regression analysis in the Origin® software package.

### 4.9. Steady-state fluorescence titrations

Fluorescence measurements were performed using a PTI C60 photon counting spectrophotometer. In a typical experiment, the porphyrin (2.0 mL, $1.0\times10^{-6}$ M) in DMSO was added to a quartz cuvette and the initial fluorescence profile of the porphyrin was recorded ($\lambda_{ex}$=415 nm for **18a** and **18b**, $\lambda_{ex}$=430 nm for **20a** and **20b**, while monitoring the fluorescence between $\lambda$=550–800 nm). Aliquots (10–20 μL) of a DMSO solution of the iron(terperidine) ($2.0\times10^{-5}$ M) were added to the cuvette while stirring. After each addition, the fluorescence spectrum was recorded. Upon reaching 1.5–2 equiv. of iron(terperidine), the aliquots were increased to 50–200 μL until 1.1 mL (8–10 equiv.) was added. The raw fluorescence intensities ($\lambda_{em}$=633 nm for **18a** and **18b**, $\lambda_{ex}$=650 nm for **20a** and **20b**) were used to generate the inverse Stern–Volmer quenching plots.

## Acknowledgements

This work was supported by the Natural Sciences and Engineering Research Council of Canada and the University of Alberta. We are grateful to Dr Randy Whittal for obtaining the mass spectral data of the complexes.

## References

1. Ward, M. D. *Chem. Soc. Rev.* **1997**, *26*, 365 and references therein.
2. Imamura, T.; Fukushima, K. *Coord. Chem. Rev.* **2000**, *198*, 133.
3. Haycock, R. A.; Yartsev, A.; Michelsen, U.; Sundstrom, V.; Hunter, C. A. *Angew. Chem., Int. Ed. Engl.* **2000**, *39*, 3616.
4. Ogawa, K.; Kobuke, Y. *Angew. Chem., Int. Ed. Engl.* **2000**, *39*, 4070.
5. Chichak, K.; Branda, N. R. *Chem. Commun.* **2000**, 1211.
6. Mak, C. C.; Bampos, N.; Sanders, J. K. M. *Chem. Commun.* **1999**, 1085.
7. Wilson, G. S.; Anderson, H. L. *Chem. Commun.* **1999**, 1539.
8. Otsuki, J.; Harada, K.; Toyama, K.; Hirose, Y.; Araki, K.; Seno, M.; Takatera, K.; Watanabe, T. *Chem. Commun.* **1998**, 1515.
9. Drain, C. M.; Nifiatis, F.; Vasenko, A.; Batteas, J. D. *Angew. Chem., Int. Ed. Engl.* **1998**, *37*, 2344.
10. Hunter, C. A.; Shannon, R. J. *Chem. Commun.* **1996**, 1361.
11. Hunter, C. A.; Hyde, R. A. *Angew. Chem., Int. Ed. Engl.* **1996**, *35*, 1936.
12. Agirtas, S.; Ion, R.-M.; Bekaroglu, O. *Mater. Sci. Engng C* **2000**, *7*, 105.
13. Kano, K.; Minamizono, H.; Kitae, T.; Negi, S. *J. Phys. Chem A* **1997**, *101*, 6118.
14. Lipskier, J. F.; Tran-Thi, T. H. *Inorg. Chem.* **1993**, *32*, 722.
15. Schneider, H.-J.; Wang, M. *J. Org. Chem.* **1994**, *59*, 7464.
16. Drain, C. M.; Shi, X.; Milic, T.; Nifiatis, F. *Chem. Commun.* **2001**, 287.
17. Masiero, S.; Gottarelli, G.; Pieraccini, S. *Chem. Commun.* **2000**, 1995.

18. Ikeda, C.; Nagahara, N.; Motegi, E.; Yoshioka, N.; Inoue, H. *Chem. Commun.* **1999**, 1759.
19. Drain, C. M.; Russell, K. C.; Lehn, J.-M. *Chem. Commun.* **1996**, 337.
20. Myles, A. J.; Branda, N. R. *J. Am. Chem. Soc.* **2001**, *123*, 177.
21. Berg, A.; Shuali, Z.; Asano-Someda, M.; Levanon, H.; Fuhs, M.; Mobius, K.; Wang, R.; Brown, C.; Sessler, J. L. *J. Am. Chem. Soc.* **1999**, *121*, 7433.
22. Osuka, A.; Yoneshima, R.; Shiratori, H.; Okada, T.; Taniguchi, S.; Mataga, N. *Chem. Commun.* **1998**, 1567.
23. Hayashi, T.; Miyahara, T.; Norihiro, K.; Tukitoshi, K.; Masuda, H.; Ogoshi, H. *J. Am. Chem. Soc.* **1997**, *119*, 7281.
24. Arimura, T.; Brown, C. T.; Springs, S. L.; Sessler, J. L. *Chem. Commun.* **1996**, 2293.
25. Kirby, J. P.; van Dantzig, N. A.; Chang, C. K.; Nocera, D. G. *Tetrahedron Lett.* **1995**, *36*, 3477.
26. Turro, C.; Chang, K.; Leroi, G. E.; Cukier, R. I.; Nocera, D. G. *J. Am. Chem. Soc.* **1992**, *114*, 4013.
27. Schmuck, C. *Chem. Eur. J.* **2000**, *6*, 709.
28. Sebo, L.; Schweizer, B.; Diederich, F. *Helv. Chim. Acta* **2000**, *83*, 80.
29. Linton, B.; Hamilton, A. D. *Tetrahedron* **1999**, *55*, 6027.
30. Bell, T. W.; Hext, N. H.; Khasanov, A. B. *Pure Appl. Chem.* **1998**, *70*, 2371.
31. Fan, E.; Van Arman, S. A.; Kincaid, S.; Hamilton, A. *J. Am. Chem. Soc.* **1993**, *115*, 369.
32. Norsten, T. B.; Chichak, K.; Branda, N. R. *Chem. Commun.* **2001**, 1794.
33. Mukkala, V.-M.; Helenius, M.; Hemmila, I.; Kankare, J.; Takalo, H. *Helv. Chim. Acta* **1993**, *76*, 1361.
34. Lindsey, J. S.; Prathapan, S.; Johnson, T. E.; Wagner, R. W. *Tetrahedron* **1994**, *50*, 8941.
35. Schaefer, J. P.; Lark, J. C.; Flegal, C. A.; Hoing, L. M. *J. Org. Chem.* **1967**, *32*, 1372.
36. de Groot, J. A.; Koek, J. H.; Lugtenburg, J. *Recl. Trav. Chim. Pays-Bas* **1981**, *100*, 405.
37. Datta-gupta, N.; Jones, E.; Thomas, L. K.; Malakar, D. *J. Indian Chem. Soc.* **1981**, *58*, 1171.
38. Suarez, M.; Salfran, E.; Rodriguez-Curiel, R. I.; Elguero, J. *Bull. Soc. Chim. Belg.* **1997**, *106*, 211.
39. Corbell, J. B.; Lundquist, J. J.; Toone, E. J. *Tetrahedron: Asymmetry* **2000**, *11*, 95.
40. Kavarnos, G. J. *Fundamentals of Photoinduced Electron Transfer*; VCH: New York, 1993.
41. Turro, N. J. *Modern Molecular Photochemistry*; University Science Books: Sausalito, 1991; pp 297–361.